Pinning of scroll waves to flat and highly branched unexcitable heterogeneities

Dhriti Mahanta,[1] Sumana Dutta,[1,*] and Oliver Steinbock[2,†]

[1]*Department of Chemistry, Indian Institute of Technology Guwahati, Guwahati 781039, India*
[2]*Department of Chemistry and Biochemistry, Florida State University, Tallahassee, Florida 32306-4390, USA*

System heterogeneities such as organelles, cells, and anatomical features strongly affect nonlinear wave patterns in biological systems. These effects are more readily studied in otherwise homogeneous chemical reactions that allow the introduction of tailored structures. Following this approach, we investigate the dynamics of three-dimensional excitation vortices pinned to inert sheets with circular holes arranged on a hexagonal lattice. Experiments with the Belousov-Zhabotinsky reaction and numerical simulations of an excitable reaction-diffusion model reveal vortex pinning that circumvents the rapid collapse of free vortex rings. The pinned scroll waves are affected by the topological mismatch between their looplike rotation backbone and the branched pinning structure. Depending on the initial condition, a multitude of stable vortex states exist, all of which obey topological constraints, suggesting spinlike states for the involved obstacle holes.

I. INTRODUCTION

Far from thermodynamic equilibrium, self-organized spatiotemporal patterns occur in a large number of reaction-diffusion systems. Among those patterns, nonlinear waves have attracted considerable interest as they are known to create stable wave pulses and surprising vortex states [1]. These rotating vortices are also ubiquitous in the realm of biology and often allow the relay of (desired or detrimental) information over macroscopic distances [2–4]. Important examples include the cellular slime mold *Dictyostelium discoideum* [5], which uses spiral waves to coordinate cell aggregation, and the human heart [6], in which rotating action potentials generate life-threatening arrhythmias [7,8]. The overwhelming number of experimental and theoretical studies of these rotors focus exclusively on spatially homogeneous, two-dimensional systems [9]. However, this premise is not valid for living systems that are typically three dimensional and intrinsically heterogeneous at both the sub- and supracellular levels.

One of the interesting consequences of heterogeneities is the possibility of vortex pinning to inert, impermeable, or electrically insulating structures. This pinning was first studied for two-dimensional spiral waves that in homogeneous media rotate around a zero-dimensional phase singularity at the center of the pattern [10]. The associated motion of the spiral tip occurs around this special point, but the tip can also be forced to follow the boundary of appropriately chosen heterogeneities as long as the size of the defect is not much smaller than the tip orbit of the free spiral [11,12]. Once pinned in such a manner, a slow translation of the anchoring heterogeneity relocates the rotating tip over potentially large distances [13,14].

In three space dimensions, the situation is more complex as the vortex rotation cannot occur around a point but is organized by a one-dimensional phase singularity. This filament can move and reshapes itself according to local speeds that are essentially proportional to the local curvature

[15]. Furthermore, filament loops shrink and disappear in all systems with a positive filament tension (a system-specific parameter) [16]. The vortex field itself is called a scroll wave and can be twisted if the rotation phase varies along the filament [17]. Scroll waves have been observed in experiments with the aforementioned slime mold and in the thick ventricles of the human heart [18,19]. In addition, they have been studied systematically in the chemical Belousov-Zhabotinsky (BZ) reaction, which is a convenient and highly reproducible model of excitable and oscillatory reaction-diffusion systems in general [20].

The three-dimensional BZ system has also been used to demonstrate and study scroll wave pinning [21–24]. This is usually accomplished by introducing inert and impermeable obstacles into the medium. To avoid undesired hydrodynamic effects and to reliably position the heterogeneities in the system, the reaction is often carried out in a gel. Using this approach, Jiménez *et al.* investigated the pinning of scroll rings to thin (complete and cut) tori [21] as well as small beads and rods [22,23]. Most of these objects can stop the curvature-controlled decay of the filament loop and thus have a profound impact on the evolution of the system. For pinning to occur, the filament of the initial scroll wave must be at least locally in close vicinity of the anchor (less than one pattern wavelength) or reach this proximity during its free motion. Once a local contact is established, the filament tends to self-wrap around the heterogeneity [23,25].

Two of us demonstrated the pinning of scroll rings to topological mismatched double tori and specifically also the pinning to one of the subtori [24]. Again pinning is possible and prevents vortex annihilation, but the wave dynamics are more complex as the rotation around the subtorus is periodically perturbed by the junction to the other, vortex-free subtorus. Accompanying simulations of the dynamics showed anchoring of scroll ring pairs to double tori for states with not only equal but also opposite chirality. In this article, we report a continuation of the latter work and demonstrate the pinning of scroll waves to planar sheets with periodically arranged holes. These inert objects are highly branched and much larger than the vortex anchors studied earlier allowing scroll wave pinning in a multitude of discrete patterns.

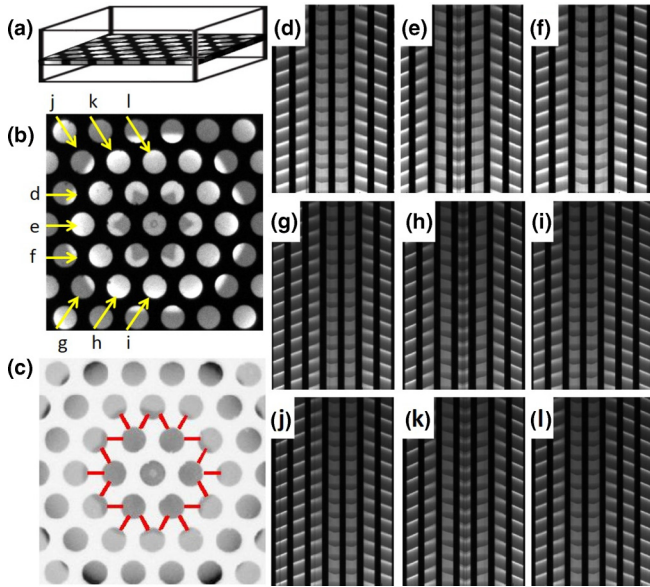*sumana@iitg.ernet.in
†steinbck@chem.fsu.edu

FIG. 1. Pinning of a three-dimensional scroll wave to an inert mesh. (a) Side view of the experimental setup, showing the flat hexagonal mesh, placed halfway between the gel. (b) Top view of a single scroll wave pinned to the thin rim around the seven central holes (bright circles). The field of view is $2.9 \times 2.9 \text{ cm}^2$. (c) The same vortex rotates through next-neighbor holes that are indicated by solid (red) lines [the color of the original snapshot in (b) has been inverted]. (d)–(l) Time-space plots generated along lines marked by the yellow arrows in (b). Time increases in the downward direction spanning 100 min. See also the movie in [27].

II. EXPERIMENTAL METHODS

We use the autocatalytic BZ reaction for our experimental study. The reaction is carried out in a Petri dish of diameter 10 cm using two BZ gel layers of thickness 4 mm each. Both layers are chemically identical and contain 0.8 % w/v agarose. The initial concentrations of the reactants in both the layers are $[\text{NaBrO}_3] = 0.04 \text{ M}$, $[\text{CH}_2(\text{COOH})_2] = 0.04 \text{ M}$, $[\text{H}_2\text{SO}_4] = 0.16 \text{ M}$, and $[\text{Fe}(\text{o-phen})_3\text{SO}_4] = 0.5 \text{ mM}$. Ultrapure water with a resistivity of $18.2 \text{ M}\Omega \text{ cm}$ is used to prepare all the solutions as well as the BZ gels. Notice that this BZ system has positive filament tension [26] and accordingly all free scroll rings shrink and vanish in finite time. The vortex pinning heterogeneity is a rigid hexagonal mesh made of a black nonreactive polymer of thickness 1.1 mm. The mesh holes are circular and have a diameter of 3.1 mm. The distance between the centers of two neighboring holes is 4.5 mm. This sheet is placed onto the lower gel layer while it is still soft and then gently pressed into it so that the forming gel covers about half of the mesh thickness. A representative cross section of the reaction chamber can be seen in Fig. 1(a). An expanding chemical wave is created by inserting the tip of a silver wire into the gel for a few seconds. The initiation process is based on the decrease in the concentration of the inhibitor bromide via formation of solid AgBr on the wire. When the wave reaches the desired diameter, the second layer is poured over the mesh with the pregel solution being slightly above the gelling temperature. Subsequently, the rim of the wave spontaneously curls into the upper layer and

creates the desired scroll wave. The system is illuminated from below by diffuse white light. A charge coupled device camera equipped with a blue dichroic filter is mounted above the reaction system and records images (640×480 pixels) at 2-s intervals. The resulting image sequences are analyzed using in-house MATLAB scripts. All experiments are carried out at room temperature.

III. EXPERIMENTAL RESULTS

Figure 1(b) shows an image of a representative wave pattern in our experimental system. The black area corresponds to the polymer mesh, while the circular areas reveal the projection of the three-dimensional wave pattern onto the image plane. Accordingly, the local intensity values are the sum of the system absorption along the vertical direction. In this particular experiment, we initiate a wave in the central hole of the mesh and before introduction of the second gel layer, allow the wave to propagate across the six adjacent holes. A time lapse video of the experiment suggests that the resulting scroll wave rotates around the outer rim of these six holes. More precisely, the vortex wave rises through the 12 holes that form the surrounding hexagon, moves inward, and then descends into the lower layer through the six holes of the inner hexagon. This circulatory motion along the rings of 6 and 12 holes is illustrated in Fig. 1(c). Each hole-connecting line in this figure is detected by computer software that analyzes the phase relation between the excitation events in neighboring holes.

The rotation pattern of this pinned vortex is further analyzed by the time-space plots in Figs. 1(d)–1(l). Each plot is generated by stacking consecutive one-dimensional intensity profiles so that time increases in the downward direction. Accordingly, a propagating wave pulse generates a bright diagonal band and the stationary polymer mesh creates vertical black lines. The different time-space plots represent the intensity dynamics along the nine lines indicated by the bright (yellow) arrows in Fig. 1(b). These diagrams allow us to distinguish between unidirectional wave propagation and rotating vorticity. The former manifests itself as a continuous diagonal line (interrupted by the dark stripes), whereas the latter tends to create fish-bone-shaped patterns because waves are emitted in alternating directions and with a typical phase difference of 180°. Finally, wave collisions can be discerned as V-shaped patterns within a single hole. For this specific experiment, the collision feature is most prominent in the central hole and hence the corresponding time-space plots in Figs. 1(e), 1(h), and 1(k). If we follow the yellow arrow e in Fig. 1(b), it cuts across seven holes separated by the dark mesh area. This is reflected in Fig. 1(e) as seven bright bands, interspersed by six thin black bands. The fish-bone structure that emanates from the second and fifth black bands in the latter points to the presence of a filament section in that region of the mesh, as is evident in Fig. 1(c). The V-shaped pattern in the central hole of this time-space plot arises out of wave collision. The rotation feature is present in all nine plots and their locations match our earlier description.

The pinned vortex shown in Fig. 1 is only one of many possible states that can be selected by initiating waves in one or more holes and by controlling their expansion time. In Fig. 2
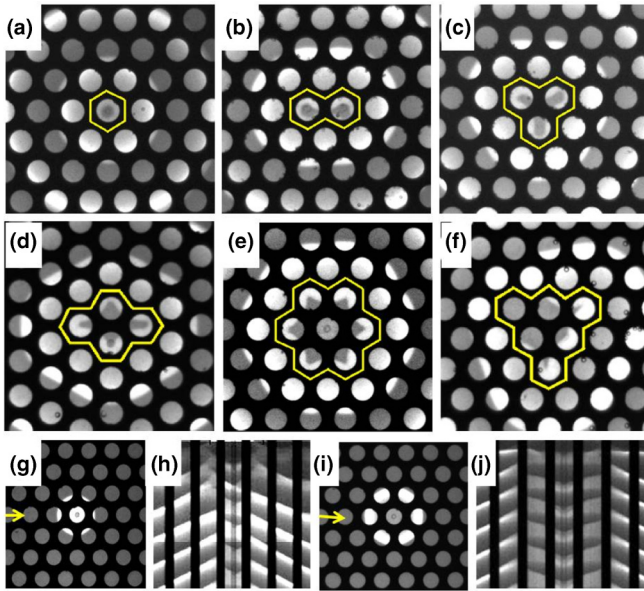
FIG. 2. Snapshots of six experiments showing scroll waves with different pinning patterns. The area of each snapshot is $2.9 \times 2.9 \, \text{cm}^2$. The yellow lines represent the shapes of the reconstructed filaments. The width-to-height ratios of the closed filaments in are (a) 1, (b) 0.55, (c) 1, (d) 0.68, (e) 1, and (f) 1. (g) and (i) Snapshots of the initial conditions giving rise to the scroll waves in (a) and (e), respectively. (h) and (j) Corresponding time-space plots illustrating the formation of the filament and its subsequent pinning. The time-space plots span a time interval of 48 min. See also the movies in [27].
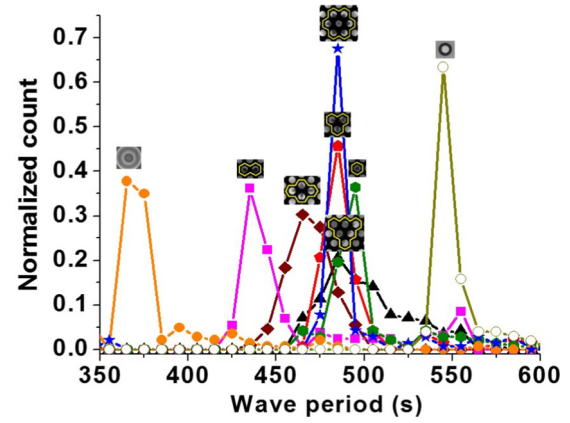

FIG. 3. Normalized distribution of wave periods of scroll waves having different filament geometries. The respective geometries are shown on the top of each curve. The closed circles (orange) show the frequency distribution of a free scroll wave and the open circles (olive) are for a circular scroll wave pinned to an O-ring. The hexagons (green), squares (magenta), pentagons (red), diamonds (wine), stars (blue), and triangles (black) represent the filaments pinned to the hexagonal mesh as shown in Figs. 2(a)–2(f), respectively.

we show six different examples (all of which we observed in at least three independent experiments) with the pattern in Fig. 2(a) being the simplest possible. The wave pattern is created from a single initiation site and its extent at the time of vortex nucleation (introduction of the top gel layer) is shown in Fig. 2(g). Its rotation occurs downward through the central hole and upward through the six surrounding ones. This behavior is also illustrated in the time-space plot in Fig. 2(h). Notice that similar initial conditions could give rise to different patterns. Figures 2(g) and 2(i) are initial conditions giving rise to the patterns in Figs. 2(a) and 2(e). In both these cases, a single hole has been excited; however, our experiments show that the smaller vortex occurs only if the vortex-initiating wave is not larger than the circle defined by the centers of the six-hole hexagon, as is the case in Figs. 2(a), 2(g), and 2(h).

Figures 2(b)–2(d) and 2(f) show pinned scroll waves that we created by simultaneous wave initiation in multiple next-neighbor holes. The vortex in Fig. 2(b) forms after two-hole initiation and its wave front descends through this pair of holes but ascends through the surrounding eight holes. Notice that the demarcation line between these hole groups is indicated as a bright (yellow) line and can be understood as the rotation backbone or equivalent of a filament. Examples of three-hole initiation are shown in Figs. 2(c) and 2(f). Here the rotation involves three and six holes, respectively. Both vortex patterns result from the same initiation configuration but different expansion times. Finally, Fig. 2(d) illustrates a four-hole case. We also note that initiation of vortices along chains of single

holes has proven difficult with the exception of two holes. The resulting wave patterns are very complicated and difficult to interpret, suggesting a breakup into several scroll rings.

The pinned scroll waves in Fig. 2 are a small selection of the large number of distinct vortex states that can be pinned to the hexagonal mesh. A trivial extension is the creation of several vortices at different locations. Such patterns do not need to be separated by large distances as their rotation patterns might even share a common hole or line of holes. Other possibilities include nested vortex states. Nonetheless, topological constraints apply such as the exclusion of branched or dangling vortex lines. We also note that for the geometric and chemical parameters studied here, we never observed that a completely pinned structure changed into another one. However, complications can arise if free filament segments exist and move under their own curvature or if filaments terminate at the upper or lower system boundary.

The anchored vortices have rotation periods that differ from the system-specific period of a free scroll wave. These rotation periods also determine and are identical to the local excitation periods in the entire wave pattern. We analyze this aspect by computing the wave period from the intensity changes in the center of every hole within the field of view. From these 150 periods, we compile the distributions shown in Fig. 3. For instance, the orange curve (closed circles) characterizes a free, slowly collapsing scroll ring. Its average is about 360 s. Doppler effects due to the slow contraction of the filament are small and possibly not resolved. All pinned vortex states have periods in the range of 430–500 s and are hence, on average, 30% larger than the value of the free scroll ring. This increase is caused by at least two factors, namely, the longer orbits enforced by the rotation around the connecting segments of the mesh and the topological frustration created by the mismatch between a filament loop and the mesh structure.

The results in Fig. 3 suggest a dependence of the period on the specific vortex type. Within the aforementioned range, the

small two-hole state [see also Fig. 2(b)] is the fastest pinned rotor, with a period of 430 s. It is followed by the four-hole rotor [see Fig. 2(d)], while all other states are close to a period of 480 s and possibly identical. Geometric parameters that could explain this ordering include the aspect ratio of the vortex line. If we consider the vortex lines to be simple polygonal curves such as those shown in Figs. 2(a)–2(f), the width-to-height ratios (width being shorter than height) are 0.55 [two holes, Fig. 2(b)], 0.68 [four holes, Fig. 2(d)], and larger values close to 1.0 for all others. We do acknowledge that the great diversity of the pinned vortices is likely to require more elaborate measures for the description of their rotation periods.

To evaluate the impact of the topological mismatch between the normal filament loop of a scroll ring and the branched structure of the mesh, we perform additional pinning experiments with a simple inert torus. The thickness of the torus (1.6 mm) is chosen to yield a circumference (5.0 mm) that matches the length of the shortest orbit available to the pinned scroll waves. The latter is determined by the shortest distance between neighboring holes (1.4 mm) and the thickness of the mesh (1.1 mm). This topologically matched pinning experiment yields a rotation period of about 550 s and is hence the longest period observed. This finding is very surprising, as one could expect the branched structure of the mesh to hinder the rotation. We also note that a qualitatively similar result was obtained in earlier experiments on single scroll rings pinned to double tori. The latter structures had a 6% shorter period than scroll waves pinned to otherwise identical single tori.

IV. MODEL AND SIMULATION METHODS

To obtain further insights into the rather complex motion of the pinned scroll waves, we performed three-dimensional numerical simulations with the Barkley model [28]. This simple, two-variable model is given by the reaction-diffusion equations

$$\frac{\partial u}{\partial t} = \frac{1}{\epsilon}\left\{u(1-u)\left(u - \frac{v+b}{a}\right)\right\} + D_u \nabla^2 u,$$

$$\frac{\partial v}{\partial t} = u - v + D_v \nabla^2 v.$$

The fast variable u and the slow variable v qualitatively describe the concentrations of $HBrO_2$ and $Fe(o\text{-phen})_3^{2+}$, respectively. Our simulations are carried out for $a = 1.1$, $b = 0.84$, $\epsilon = 0.02$, and diffusion constants of $D_u = D_v = 1.0$. These parameters describe an excitable system with positive filament tension. Explicit Euler integration and a seven-point Laplacian stencil are used to numerically solve the two partial differential equations. The integration time step is kept constant at 0.012. Our simulations employ a three-dimensional lattice of $320 \times 320 \times 200$ grid points with a grid spacing of 0.35. The unexcitable mesh is modeled as a continuous domain with the approximate shape of the experimental mesh and Neumann boundaries to the surrounding excitable medium. These no-flux boundary conditions match the impermeable character of the polymer sheet in the experiments and fully block wave propagation. The hole diameter and spacing are 14 and 16.8 space units, respectively. The thickness of the mesh is 1.4 space units. A no-flux boundary condition is also set for each diffusing species along the external boundaries. The filament of the scroll wave is identified as regions where $u = 0.5$ and $v = a/2 - b$. Following the initiation of the desired scroll wave, transients in our simulations are minor and short lived. The reported wave patterns and filaments represent the stationary rotation patterns of the pinned vortices. Our simulations extended over time intervals during which the pinned vortex performed at least 80 rotation cycles. A free
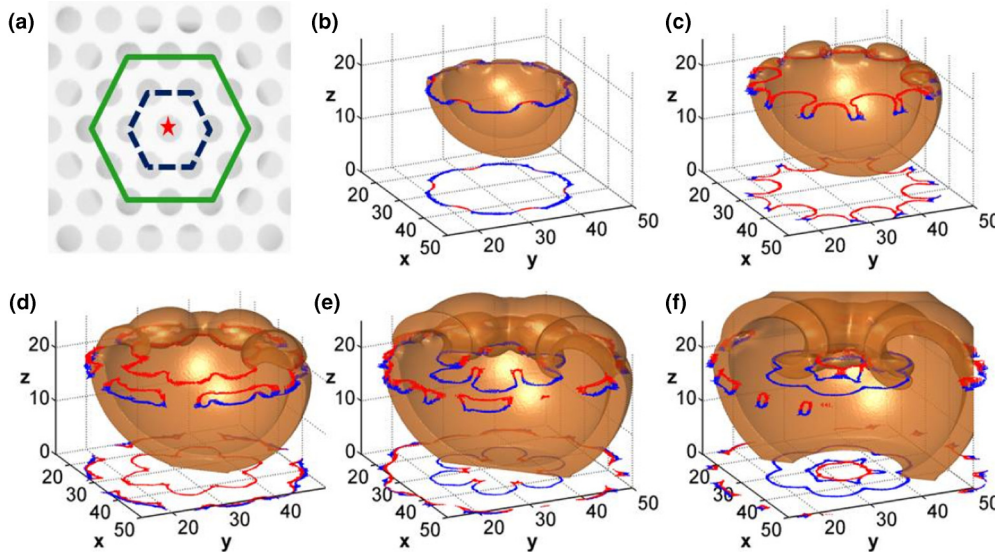

FIG. 4. Numerical simulation of the dynamics of a scroll wave pinned to the rim around the seven central holes. (a) Snapshot of the mesh (white) showing the hexagonal inner ring r_1 (dashed blue line) and outer ring r_2 (solid green line) around the central hole (red star). (b)–(f) Evolution of the wave pattern (solid brown areas) and the filament (red and blue curves). Filament sections above the central horizontal plane ($z = 20$) are indicated by red curves, while blue curves depict those below the plane. The two-dimensional projections of the filaments are shown at the bottom of the box ($z = 0$). Time intervals between neighboring frames are 1.7, 1.2, 1.2, and 1.0 time units. The computed volume has been cropped along the boundaries.

scroll ring of size comparable to the example in Fig. 1 would have collapsed in 24 cycles.

V. SIMULATION RESULTS

Figure 4 summarizes the results of a typical simulation. The images in Figs. 4(b)–4(f) illustrate the evolution of a three-dimensional scroll wave pinned to an unexcitable layer [see Fig. 4(a)]. The specific case in Fig. 4 is analogous to the experiment shown in Fig. 1. Orange regions ($v > 0.4$) indicate that the system is locally excited, whereas transparent areas are either refractory or newly excitable. We omit the three-dimensional obstacle and only show the posterior half of the vortex, for better visualization. The circulatory wave activity is seen to concentrate around two hexagonal structures: an inner ring of six holes that encircles the central hole and an outer ring of 12 holes that encircles these seven holes [Fig. 4(a)]. Figure 4(b) shows an early stage of the simulation that is similar to the initial experimental condition, i.e., a semispherical wave in the lower gel layer. This bowl-shaped structure starts curling up into the top layer through the outer ring [Figs. 4(c) and 4(d)] and descends through the ring of inner holes [Figs. 4(e) and 4(f)]. Every time a wave segment emerges from a hole it collides with wave segments from the neighboring holes, creating a segmented rim structure. Also note that the wave temporarily loses contact when turning around the sharp edges of the heterogeneity.

Near the rotation-controlling holes, the line of contact between the wave and the obstacle is closely related to the filament of the vortex and in the following we will refer to it as the filament. In Fig. 4, filament segments above (below) the central plane are plotted in red (blue). The entire filament is also projected onto the $z = 0$ plane, maintaining the aforementioned color coding. In Figs. 4(b) and 4(c), the filament is turning upward and acquires 12 Ω-shaped features that correspond to the 12 holes of the outer ring. Due to the obstacles between the holes, parts of the filament stay below the mesh [blue parts in Fig. 4(c)]. Subsequently, these segments detach from the main loop and move outward. A similar process occurs above the mesh and sheds additional (red) filament segments [Fig. 4(d)]. These red and blue parts form connected entities [Figs. 4(e) and 4(f)] and move outward but are not associated with sustained wave rotation (see also movie 4 in [27]). This complicated process is the direct consequence of the topological frustration in this system, which does not allow uninterrupted rotation. Finally, the now rather small main loop begins to ascend between Figs. 2(e) and 2(f) to complete the rotation cycle.

The shape of the filament in Fig. 4(d) closely resembles the suggested vortex line of the experimental result shown in Fig. 2(e). Figure 5 provides additional numerical examples that were constructed from identical simulations but different initial conditions and/or expansion times. From top to bottom, the four rows correspond to scroll waves pinned to inner rings containing two, three, four, and six holes. Each row shows the filament at four different phases. Again we find good qualitative agreement with the vortex lines in Fig. 2. We suggest that these shapes are widely independent of the model and also the experimental system as they primarily depend on a steady spread of the wave and not subtle dynamic features.
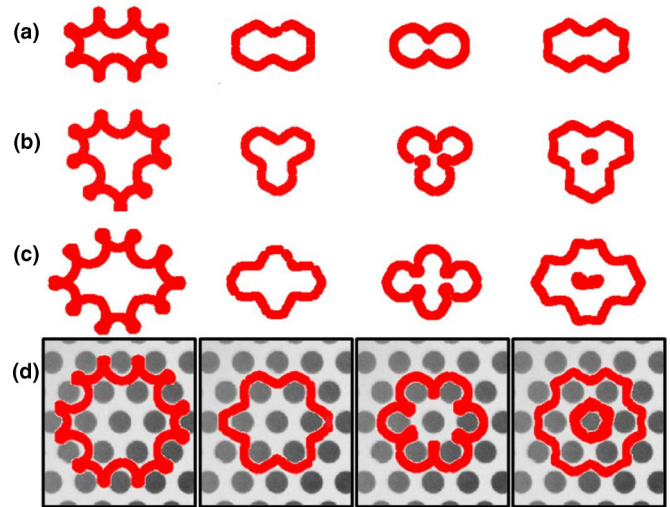

FIG. 5. Numerical simulations of filament shapes and dynamics for scroll waves pinned to a hexagonal mesh. (a)–(d) Each row shows the filament at four different phases. The rows differ only in the initial conditions that were employed during the simulations. In (d) the filament is shown as a projection over the hexagonal mesh structure. The results are similar to the experiments in Figs. 2(b)–2(e).

VI. DISCUSSION AND CONCLUSION

We have shown that vortex structures can be readily pinned to a thin planar heterogeneity containing a periodic array of holes sufficiently large to allow the reliable passage of excitation waves. The pinning prevents the collapse of the scroll waves and creates a very large number of possible vortex states that in principle encode and store information by assigning an up (+) or down (−) direction to particular holes participating in the vortex's rotation pattern. All holes that are not part of this pattern are essentially unassigned entities. This binary (or trinary) information storage in a dynamical system is subject to strict topological rules that are not as obvious as those ruling the filaments of free scroll waves. Furthermore, the hole charges are generating vortex lines that in our simulations are readily detected and in the experiments deducible from the wave's local excitation phase. These lines exist between all neighboring holes with opposite charge and can be assigned a direction according to the rotation direction of the waves.

Figure 6 illustrates these features for several examples by assigning the aforementioned charges to the participating holes and vortex lines with directions selected according to the right-hand rule. For example, the upper left vortex pattern is a simple one-hole vortex with an outer ring of six holes. Notice that the same pattern can exist with reversed charges and line directions. Next to it is a two-hole rotor similar to those shown in Figs. 2(b) and 5(a). The inner hole pair has the same charge and accordingly two vortex lines of opposing direction could be drawn but cancel in the context of our interpretation giving rise to a simple unbranched vortex line. Below we show as a third example a vortex with six inner holes and nonparticipating central hole to illustrate that the inside of large vortices may have a charge of zero.

Under the rules of this method, we can assign arbitrary combinations to the grid holes and generate the corresponding
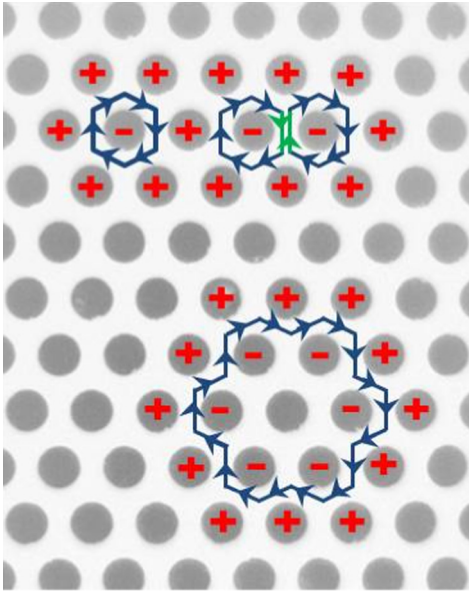
FIG. 6. Schematic drawing illustrating our interpretation of pinned vortices in terms of topological charges and derived filaments. The local charges $+$ and $-$ represent the upward or downward motion of the excitation wave through the given hole, respectively. Filaments are shown as (blue) bold lines with arrows marking their directionality in accordance with the right-hand rule. Two neighboring vortices can share a common hole and oppositely directed filament segments (green) cancel each other.

vortex lines. Some of these combinations can be expected to be unstable as our experiments did not support the creation of pinned vortices with a line of three or more next-neighbor inner holes. Moreover, specific initial conditions in the actual experiment or simulation can create bidirectional wave passage through given holes. For example, one could initiate an upward moving wave pulse in one hole and a downward moving front in a next neighbor hole. This situation should result in bidirectional wave motion in the two holes closest to the pair where the waves were initiated. Two of us studied a similar scenario in earlier experiments with a double torus where the pinning of two scroll rings with opposite hole-passage direction induced a complicated two-armed vortex at the junction [24]. Clearly more work is needed to evaluate this and related configurations for the extended mesh.

Many other experiments can be envisioned for similar heterogeneities including nonuniform hole sizes. This case should be particularly interesting if some of the holes are sufficiently small to block wave passage according to firing sequences such as passage followed by blockage (1:1) or more complex sequences [29,30]. Other more obvious variations should explore different arrangements of the holes including square patterns and nested vortices. More ambitious possibilities include three-dimensional versions of the blocking heterogeneity and even dynamic ones. For biological applications, another area of interest is random heterogeneities.

In experiments with a three-dimensional chemical system and numerical simulation based on a simple mathematical model, we have shown that vortices of different shapes can be made to pin to a heterogeneous obstacle with numerous branching points. The shape of the filament depends upon the initial size of the waveform and its proximity to the nearest heterogeneities. This study could illuminate the phenomenon of pinning of scroll waves to scar tissues and other complex unexcitable structures in the cardiac system.

ACKNOWLEDGMENTS

[1] I. R. Epstein and J. A. Pojman, *An Introduction to Nonlinear Chemical Dynamics: Oscillations, Waves, Patterns, and Chaos* (Oxford University Press, New York, 1998).

[2] Y. Yu, L. M. Santos, L. A. Mattiace, M. L. Costa, L. C. Ferreira, K. Benabou, A. H. Kim, J. Abrahams, M. V. L. Bennett, and R. Rozental, Proc. Natl. Acad. Sci. USA **109**, 2585 (2012).

[3] X. Huang, W. Troy, Q. Yang, H. Ma, C. Laing, S. Schiff, and J.-Y. Wu, J. Neurosci. **24**, 9897 (2004).

[4] J. Lechleiter, S. Girard, E. Peralta, and D. Clapham, Science. **252**, 123 (1991).

[5] O. Steinbock, F. Siegert, S. C. Müller, and C. J. Weijer, Proc. Natl. Acad. Sci. USA **90**, 7332 (1993).

[6] E. M. Cherry and F. H. Fenton, New J. Phys. **10**, 125016 (2008).

[7] J. Jalife, M. Delmar, J. Anumonwo, O. Berenfeld, and J. Kalifa, *Basic Cardiac Electrophysiology for the Clinician*, 2nd ed. (Wiley-Blackwell, Oxford, 2009).

[8] R. A. Gray, J. Jalife, A. V. Panfilov, W. T. Baxter, and C. Cabo, Science **270**, 1222 (1995).

[9] R. Kapral and K. Showalter, *Chemical Waves and Patterns* (Kluwer, Dordrecht, 1995).

[10] A. T. Winfree, Science **175**, 634 (1972).

[11] O. Steinbock and S. C. Müller, Phys. Rev. E **47**, 1506 (1993).

[12] Z. Y. Lim, B. Maskara, F. Aguel, R. Emokpae, and L. Tung, Circulation **114**, 2113 (2006).

[13] O. Steinbock and S. C. Müller, Physica A **188**, 61 (1992).

[14] H. Ke, Z. Zhang, and O. Steinbock, Phys. Rev. E **91**, 032930 (2015).

[15] J. P. Keener and J. J. Tyson, SIAM Rev. **34**, 1 (1992).

[16] V. N. Biktashev, A. V. Holden, and H. G. Zhang, Philos. Trans. R. Soc. A **347**, 611 (1994).

[17] A. S. Mikhailov, A. V. Panfilov, and A. N. Rudenko, Phys. Lett. A **109**, 246 (1985).

[18] F. Siegert and C. J. Weijer, Proc. Natl. Acad. Sci. USA **89**, 6433 (1992).

[19] M. Gotoh, T. Uchida, W. J. Mandel, M. C. Fishbein, P. Chen, and H. S. Karagueuzian, Circulation **95**, 2141 (1997).

[20] W. Jahnke, C. Henze, and A. T. Winfree, Nature (London) **336**, 662 (1988).

[21] Z. A. Jiménez, B. Marts, and O. Steinbock, Phys. Rev. Lett. **102**, 244101 (2009).

[22] Z. A. Jiménez and O. Steinbock, Phys. Rev. Lett. **109**, 098301 (2012).

[23] Z. A. Jiménez and O. Steinbock, Phys. Rev. E **86**, 036205 (2012).

[24] S. Dutta and O. Steinbock, J. Phys. Chem. Lett. **2**, 945 (2011).

[25] Z. Zhang and O. Steinbock, New J. Phys. **18**, 053018 (2016).

[26] T. Bánsági, Jr. and O. Steinbock, Phys. Rev. Lett. **97**, 198301 (2006).

[27] See Supplemental Material at http://link.aps.org/supplemental/10.1103/PhysRevE.95.032204 for movies of typical experiments (corresponding to Figs. 1 and 2) and simulations (corresponding to Fig. 4).

[28] D. Barkley, Physica D **49**, 61 (1991).

[29] A. Toth, V. Gaspar, and K. Showalter, J. Phys. Chem. **98**, 522 (1994).

[30] B. T. Ginn and O. Steinbock, Phys. Rev. Lett. **93**, 158301 (2004).